X-linked susceptibility to mycobacteria is caused by mutations in NEMO impairing CD40-dependent IL-12 production

Orchidée Filipe-Santos,[1] Jacinta Bustamante,[1] Margje H. Haverkamp,[10,12] Emilie Vinolo,[2] Cheng-Lung Ku,[1] Anne Puel,[1] David M. Frucht,[11] Karin Christel,[1] Horst von Bernuth,[1] Emmanuelle Jouanguy,[1] Jacqueline Feinberg,[1] Anne Durandy,[3] Brigitte Senechal,[9] Ariane Chapgier,[1] Guillaume Vogt,[1] Ludovic de Beaucoudrey,[1] Claire Fieschi,[1,13] Capucine Picard,[1,4] Meriem Garfa,[5] Jalel Chemli,[14] Mohamed Bejaoui,[15] Maria N. Tsolia,[17] Necil Kutukculer,[18] Alessandro Plebani,[19] Luigi Notarangelo,[19] Christine Bodemer,[6] Frédéric Geissmann,[9] Alain Israël,[8] Michel Véron,[2] Maike Knackstedt,[20] Ridha Barbouche,[16] Laurent Abel,[1] Klaus Magdorf,[20] Dominique Gendrel,[21] Fabrice Agou,[2] Steven M. Holland,[10] and Jean-Laurent Casanova[1,7]

[1]Laboratory of Human Genetics of Infectious Diseases, University of Paris René Descartes-Institut National de la Santé et de la Recherche Médicale (INSERM) U 550, Necker Medical School; [2]Laboratory of Enzymatic Regulation of Cellular Activities, URA 2185 Centre National de la Recherche Scientifique (CNRS), Pasteur Institute; [3]Laboratory of Normal and Pathologic Development of the Immune System, INSERM U768, [4]Center for the Study of Primary Immunodeficiencies, [5]Laboratory of Confocal Microscopy, [6]Dermatology Unit, and [7]Pediatric Hematology-Immunology Unit, Necker Hospital; [8]Laboratory of Molecular Signaling and Cellular Activation, URA 2582 CNRS, Pasteur Institute; and [9]INSERM, Laboratory of Mononuclear Phagocyte Biology, Avenir Team, Necker Enfants Malades Institute, 75015 Paris, France
[10]Laboratory of Clinical Infectious Diseases, National Institutes of Health and [11]Laboratory of Cell Biology, Division of Monoclonal Antibodies, Center for Drug Evaluation and Research, Food and Drug Administration, Bethesda, MD 20892
[12]Department of Infectious Diseases, Leiden University Medical Center, 2300 Leiden, Netherlands
[13]Laboratory of Immunology, Saint Louis Hospital, 75010 Paris, France
[14]Department of Pediatrics, Sahloul Hospital, 4054 Sousse, Tunisia
[15]National Center for Bone Marrow Transplantation and [16]Department of Immunology, Pasteur Institute, 1002 Tunis, Tunisia
[17]Second Department of Pediatrics, University of Athens School of Medicine, P. and A. Kyriakou Children's Hospital, 115 27 Athens, Greece
[18]Department of Pediatrics, Ege University, 35100 Izmir, Turkey
[19]Department of Pediatrics and Institute for Molecular Medicine Angello Nocivelli, University of Brescia, 25121 Brescia, Italy
[20]Department of Pediatric Pulmonology and Immunology, Charité, Campus Virchow Klinikum, 13353 Berlin, Germany
[21]Department of Pediatrics, St. Vincent de Paul Hospital, 75014 Paris, France

CORRESPONDENCE
Jean-Laurent Casanova:
casanova@necker.fr

Abbreviations used: EM, environmental mycobacteria; LZ, leucine zipper; MDDC, monocyte-derived dendritic cell; MSMD, Mendelian susceptibility to mycobacterial diseases; NEMO, NF-κB essential modulator; XR, X-linked recessive.

O. Filipe-Santos and J. Bustamante contributed equally to this work.
S.M. Holland and J.-L. Casanova contributed equally to this work.

Germline mutations in five autosomal genes involved in interleukin (IL)-12–dependent, interferon (IFN)-γ–mediated immunity cause Mendelian susceptibility to mycobacterial diseases (MSMD). The molecular basis of X-linked recessive (XR)–MSMD remains unknown. We report here mutations in the leucine zipper (LZ) domain of the NF-κB essential modulator (NEMO) gene in three unrelated kindreds with XR-MSMD. The mutant proteins were produced in normal amounts in blood and fibroblastic cells. However, the patients' monocytes presented an intrinsic defect in T cell–dependent IL-12 production, resulting in defective IFN-γ secretion by T cells. IL-12 production was also impaired as the result of a specific defect in NEMO- and NF-κB/c-Rel–mediated CD40 signaling after the stimulation of monocytes and dendritic cells by CD40L-expressing T cells and fibroblasts, respectively. However, the CD40-dependent up-regulation of costimulatory molecules of dendritic cells and the proliferation and immunoglobulin class switch of B cells were normal. Moreover, the patients' blood and fibroblastic cells responded to other NF-κB activators, such as tumor necrosis factor-α, IL-1β, and lipopolysaccharide. These two mutations in the NEMO LZ domain provide the first genetic etiology of XR-MSMD. They also demonstrate the importance of the T cell– and CD40L-triggered, CD40-, and NEMO/NF-κB/c-Rel–mediated induction of IL-12 by monocyte-derived cells for protective immunity to mycobacteria in humans.

The Journal of Experimental Medicine

Mendelian susceptibility to mycobacterial diseases (MSMD) (MIM 209950) is a congenital syndrome resulting in predisposition to clinical disease caused by weakly virulent mycobacterial species, such as BCG vaccines and nontuberculous, environmental mycobacteria (EM) (1–4). Patients are also susceptible to the more virulent species *Mycobacterium tuberculosis* (5). Diseases caused by nontyphoidal *Salmonella* serotypes have been observed in just under half the cases (4). Other infectious diseases have only rarely been reported, mostly in single patients. A few patients have suffered from viral infections, including cytomegalovirus and human herpes virus-8 infections, and others have had fungal infections with species such as *Histoplasma capsulatum* and *Paracoccidioidomyces braziliensis*. MSMD was initially thought to be autosomal recessive in most, if not all kindreds, as a result of the high frequency of both multiple-case sibships and consanguineous kindreds (2, 3).

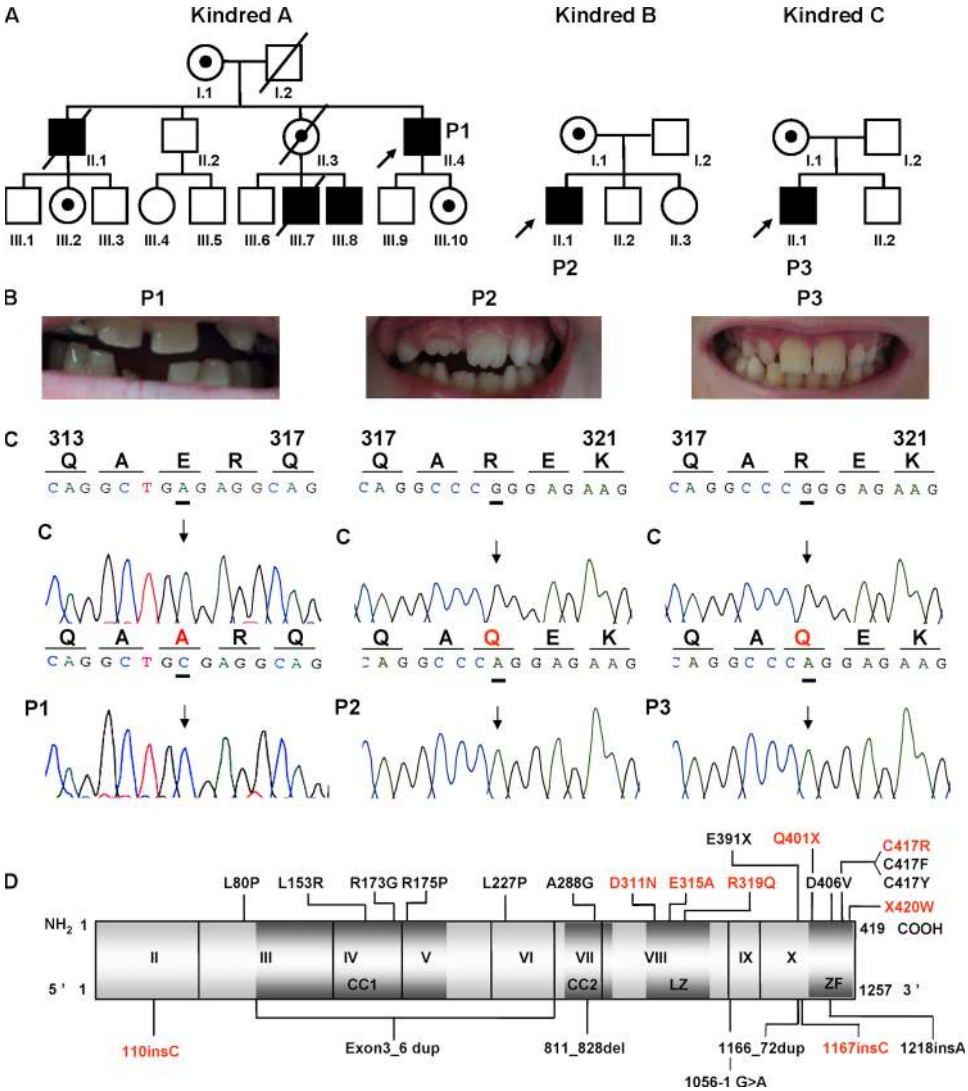

Figure 1. Clinical phenotypes and *NEMO* genotypes of patients. (A) Pedigrees of three kindreds with *NEMO* mutations (A, B, and C). Each generation is designated by a Roman numeral, and each individual is designated by an Arabic numeral. Male patients (in black squares) present mycobacterial infections and hemizygous *NEMO* mutations; asymptomatic female carriers are represented by black dots. The probands are indicated by arrows. (B) The teeth of patient P1 (Kindred A, II.4, sparse teeth), patient P2 (Kindred B, II.1, conical decidual incisors), and patient P3 (Kindred C, II.1, normal teeth). (C) Sequence electrophoregram of *NEMO* complementary DNA in the region corresponding to the mutation. Kindred A, P1 presents the mutation A→C leading to the replacement at residue 315 of Glu (E) by Ala (A) (E315A). Kindred B, P2 and kindred C, P3 present the mutation G→A resulting in the replacement of an Arg (R) at position 319 by Gln (Q) (R319Q). (D) Schematic representation of the NEMO coding region, from exons 2 to 10, and corresponding domains, shown in dark gray: the coil-coiled domain 1 (CC1, Leu 93 to Gln 194) and coil-coiled domain 2 (CC2, Met 258 to Lys 292), and the leucine zipper (LZ, Tyr 308 to Lys 344) and zinc finger (ZF, Cys 397 to Cys 417) domains. All published hypomorphic *NEMO* mutations (associated with the various forms of EDA-ID) are represented (reference 43). Missense and nonsense mutations (amino-acid code) are shown on top, whereas splice and frameshift mutations (nucleotide code) are shown on the bottom. NEMO mutations in red represent mutations associated with mycobacterial infections.

After the identification in 1996 of germline mutations in *IFNGR1*, encoding the IFN-γ receptor ligand-binding chain (IFN-γR1) (6, 7), recessive mutations were reported in three other autosomal genes: *IFNGR2*, encoding the accessory chain of the IFN-γ receptor (8); *IL12B*, encoding the p40 subunit shared by IL-12 and IL-23 (9); and *IL12RB1*, encoding the β1 chain shared by the receptors for IL-12 and IL-23 (10, 11). Defects in *IFNGR1* and *IFNGR2* are associated with impaired cellular responses to IFN-γ, whereas defects in *IL12B* and *IL12RB1* are associated with impaired IFN-γ production. Allelic heterogeneity at these four loci accounts for the existence of nine autosomal recessive disorders. After the identification of complete defects in which no protein is expressed (6–8, 10, 11), partial forms of IFN-γR1 (12) and IFN-γR2 (13) deficiency and complete forms of IFN-γR1 (14), IFN-γR2 (15), and IL-12Rβ1 (16) deficiency with surface receptor expression were identified.

The identification of MSMD-causing recessive alleles in these four autosomal genes led to the discovery of an autosomal dominant form of MSMD, caused by dominant-negative alleles of *IFNGR1* (17). The mutant alleles exert a dominant-negative effect as the result of overexpression, at the cell surface, of truncated chains that cannot transduce signals. Dominant mutations in *STAT1,* another autosomal gene encoding the signal transducer and transactivator of transcription 1 (Stat-1), were subsequently identified (18). There are two forms of partial Stat-1 deficiency, depending on whether the mutation impairs the phosphorylation of Tyr 701 (18) or DNA-binding activity (unpublished data). The two forms of partial Stat-1 deficiency are associated with MSMD because these mutations affect the activation of IFN-γ–induced Stat-1 homodimers, but not of IFN-α/β–induced Stat-1-Stat-2-IRF-9 trimers, in heterozygous cells. A dominant-negative mutant allele of *IFNGR2* has also been identified, resulting in the aberrant subcellular distribution of IFN-γR2, as the result of a mutation affecting the transmembrane domain (19).

In one family first reported in 1991, and more extensively in 1994, it was suggested that MSMD might display X-linked recessive inheritance (1, 20–22). Four maternally related male patients were found to suffer from severe EM disease. These patients' monocytes were found to be intrinsically unable to produce normal levels of IL-12 upon stimulation by PHA and T cells (21, 22). Despite the identification of this immunological phenotype, the molecular basis of XR-MSMD has remained elusive. We report here the identification of MSMD-causing *NEMO* mutations in this kindred and in two other, unrelated kindreds. These mutations do not affect NF-κB activation in response to most classical activators tested, accounting for the narrow spectrum of infections in patients. The two NF-κB essential modulator (NEMO) mutations identified selectively impair the CD40-triggered and NF-κB/c-Rel–mediated induction of IL-12 production by monocytes and monocyte-derived dendritic cells, accounting for the susceptibility to mycobacteria.

RESULTS

New germline mutations in *NEMO* in three kindreds

We studied an American multiplex kindred, a French kindred, and a German kindred, each containing one male patient with sporadic mycobacterial disease (Fig. 1 A). None of the six patients in these kindreds displayed the classical developmental and infectious features of anhidrotic ectodermal dysplasia with immunodeficiency (EDA-ID) (23–25). Conical incisors in one proband (P2, kindred B, Fig. 1 B) and in a second patient (patient III.8, kindred A) nevertheless led us to study the X-linked EDA-ID–causing *NEMO* gene (26) (unpublished data). New mutations were found in the coding region of *NEMO* in the three probands (Fig. 1 C). P1 from kindred A presented a nucleotide substitution at position 944 (A→C) (Fig. 1 C, left), leading to the replacement of a Glu by an Ala at residue 315 (E315A) (Fig. 1 D). P2 and P3 from kindreds B and C, respectively, presented a nucleotide substitution at position 956 (G→A) (Fig. 1 C, middle

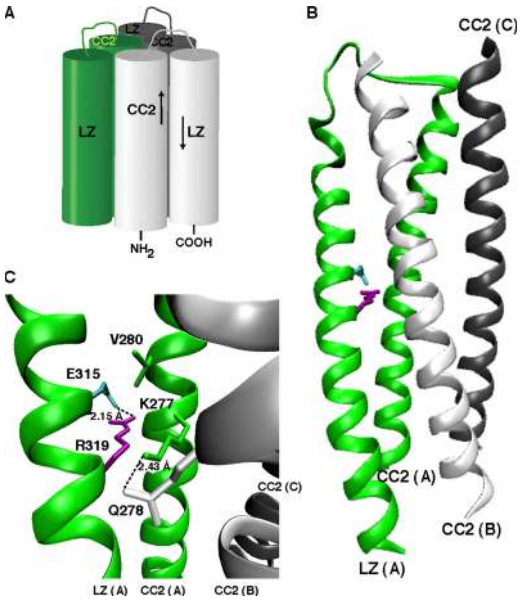

Figure 2. A model of the three-dimensional structure of NEMO. (A) Schematic representation of the structural model of the NEMO oligomerization domain. The oligomerization domains from three NEMO subunits are represented in green, light gray, and dark gray. The LZ motifs dock in an antiparallel manner in the crevices defined by the central trimeric CC2 coiled-coil. (B) Modeling of NEMO oligomerization domain. Modeling was based on the coordinates of the HIV-1 gp41 ectodomain, as described in Materials and methods. For the sake of simplicity, only one LZ domain (*LZ[A]*, in green) is represented, together with the three CC2 motifs forming the core of the pseudo-six-helix bundle. Amino acids E315 and R319, mutated in the NEMO protein of the XR-MSMD patients and located within the LZ motif, are shown in blue and purple, respectively. (C) A close-up of the surrounding environment of E315 (blue) and R319 (purple) amino acids, which probably form an intramolecular salt bridge. Spatially close to these two residues, V280 and K277 (green) are located within the CC2 motif of the same NEMO subunit. Q278 (light gray), located within the CC2 motif of the adjacent B subunit (*CC2[B]*) probably forms an intermolecular hydrogen bond with K277.

and right) resulting in the replacement of an Arg by a Gln at position 319 (R319Q) (Fig. 1 D). The two mutations were detected in cDNAs, indicating that they corresponded to *NEMO* and not the nearby *NEMO* pseudogene (27). These mutations were not found in 800 unrelated healthy controls (1,200 X chromosomes) from 51 ethnic groups (HGDP-CEPH database). The familial segregation of *NEMO* in kindred A was consistent with linkage between the observed syndrome and this gene (unpublished data). The heterozygous grandmother (I.1), and three other women in kindred A (II.3, III.2, III.10), like the mother of P2 in kindred B (I.1) and the mother of P3 in kindred C (I.1), were obligate carriers, but displayed no signs of incontinentia pigmenti or EDA (unpublished data). These data suggest that these three unrelated families suffer from XR-MSMD as the result of missense mutations in *NEMO*.

Modeling of the molecular environment of the E315 and R319 residues

Amino acids E315 and R319 are both located within the leucine zipper (LZ) domain of NEMO (Fig. 1 D). Several studies have shown that NEMO self-assembles into trimers (28, 29). The minimal oligomerization domain of the protein consists of the CC2 and LZ coiled-coil motifs, and we recently suggested that these motifs interact to form a pseudo-six-helix bundle, in which the LZ α-helices dock in the crevices defined by two of the helices of the central trimeric CC2 coiled-coil (Fig. 2 A) (30). A similar scaffold was described for the HIV-1 gp41 protein (31). We therefore modeled the NEMO trimeric CC2-LZ domain based on the X-ray structure of the gp41 ectodomain (Fig. 2 B). In our model, the E315 and R319 residues, located in the middle of the LZ domain, face the interior of the coiled coil assembly. The environment of the two residues is shown in greater detail in Fig. 2 C. E315 and R319 probably form an intramolecular salt bridge stabilizing the LZ α-helix. Other amino acids located in the vicinity of these residues in the model are also shown, including K277, from the same NEMO subunit, and Q278 from the CC2 motif of an adjacent subunit, which probably interact via a hydrogen bond. The E315A and R319Q mutations found in XR-MSMD patients would break the predicted salt bridge and might induce local plasticity in the LZ helices of the NEMO trimer. Within the highly structured CC2-LZ trimer, this might also result in local modifications to interactions with the central CC2 domains. Our structural model therefore also provides a rationale for the remarkable similarity and narrowness of the clinical phenotypes of the patients described, with *NEMO* mutations disrupting a common salt bridge in the LZ domain.

Normal expression of NEMO protein in blood cells and fibroblasts

We assessed NEMO expression by Western blotting extracts of EBV-transformed B cells and SV40-transformed fibroblasts with p18 and 3328 antibodies, which recognize the N-terminal region of NEMO. The mutant proteins, E315A

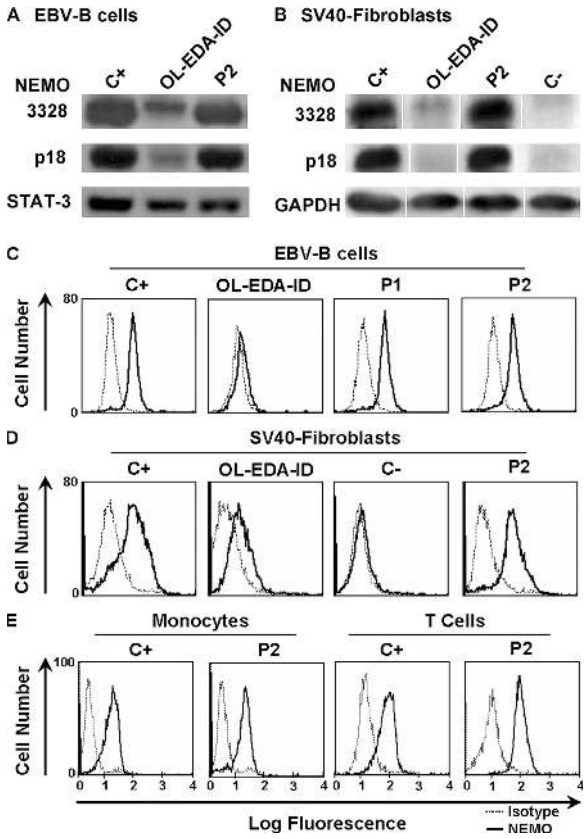

Figure 3. Expression of NEMO in the patients. NEMO protein, detected by Western blotting with two specific antibodies, 3328 and p18, which recognize different parts of the N-terminus of NEMO (A) EBV-transformed B cell lines and (B) SV-40–transformed fibroblastic cell lines from a healthy donor (C+), an OL-EDA-ID patient carrying the X420W NEMO mutation, P2 and an SV-40–transformed fibroblastic cell line from a NEMO-deficient fetus as a negative control (C−). Intracellular staining of NEMO with a specific antibody recognizing amino acids 278–396 and detected by flow cytometry in (C) EBV-transformed B cell lines and (D) SV40-transformed fibroblastic cell lines from healthy control (C+), an OL-EDA-ID patient, P1 and P2. (E) Purified monocytes (left) and T cells (right) from a healthy control (C+) and P2.

(P1) (not depicted) and R319Q (P2), were expressed in similar amounts to wild-type NEMO in EBV-transformed B cells (Fig. 3 A). The R319Q protein was also expressed in normal amounts in SV40-transformed fibroblasts from P2 (Fig. 3 B). Cell lines from P3 (R319Q) and fibroblasts from P1 (E315A) were not available. The NEMO X420W mutant, which causes the most severe form of EDA-ID (24), with osteopetrosis and lymphoedema (OL-EDA-ID), was detected only in trace amounts, at a higher molecular weight, on Western blots of EBV-transformed B cells and SV40-transformed fibroblasts (Fig. 3, A and B). As a negative control (C−) (Fig. 3 B), no NEMO was detected in SV40-transformed fibroblasts bearing a large amorphic deletion in *NEMO* (27). We assessed intracellular NEMO expression by flow cytometry, using antibody 278–396, which recognizes the C-terminal region of NEMO (32). NEMO was normally

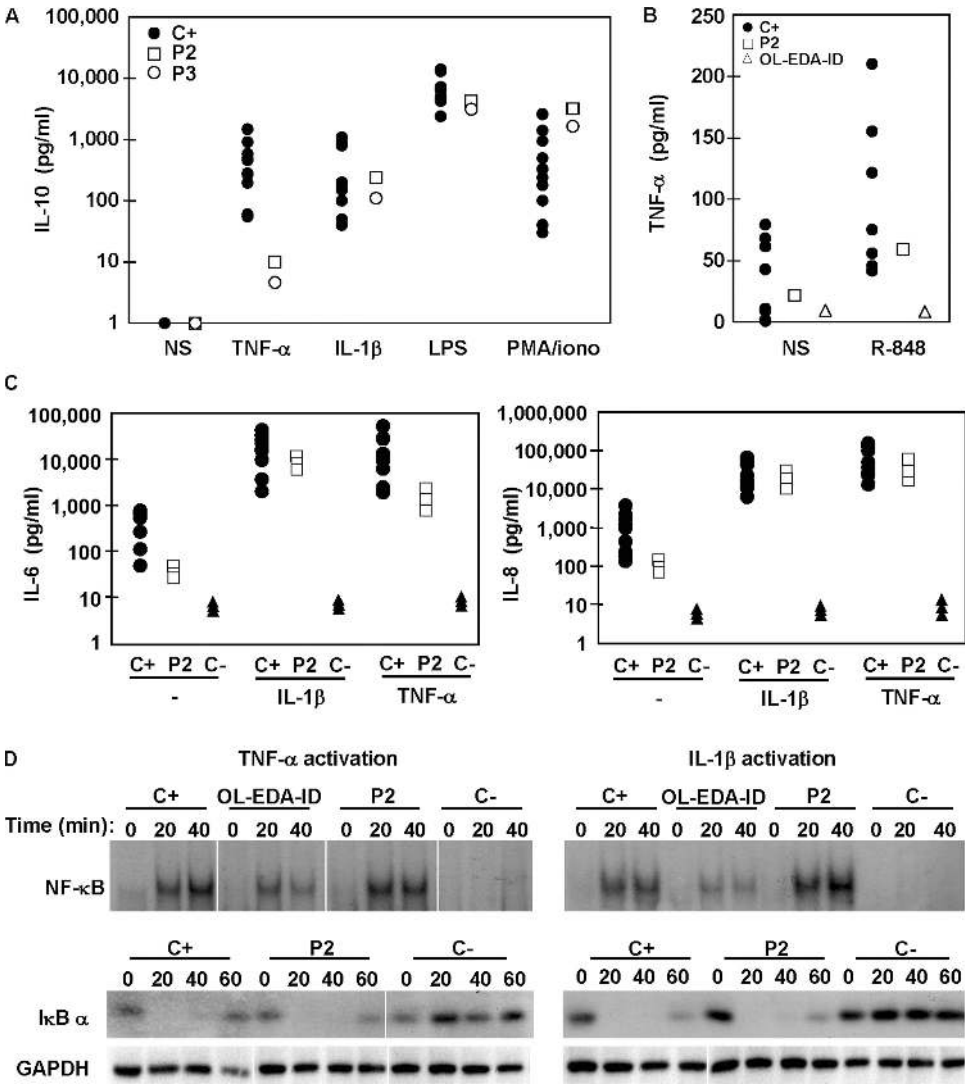

Figure 4. NF-κB activation in leukocytes and fibroblasts. Healthy controls (C+, ●), OL-EDA-ID patient (△), SV-40–transformed fibroblastic cell line from NEMO-deficient fetus (C−,▲), P2 (□), and P3 (○). (A) IL-10 production by whole blood cells from 10 healthy controls and P2 and P3, upon stimulation with LPS (1 μg/ml), TNF-α (20 ng/ml), IL-1β (10 ng/ml), and PMA/ionomycin (10^{-7}/10^{-5} M) for 48 h. (B) TNF-α production by EBV-transformed B cells after 24 h of TLR7/8 activation by R-848 agonist. (C) IL-6 and IL-8 production by SV-40–transformed fibroblastic cell lines from nine healthy controls and from P2 and C− (three experiments each for P2 and C−), after 24 h of TNF-α and IL-1β stimulation. All cytokines were determined by sandwich ELISA. (D) DNA-binding activity in nuclear extracts from fibroblastic cell lines after TNF-α (20 ng/ml) and IL-1β (10 ng/ml) activation for various lengths of time, as detected with a radio-labeled DNA probe by EMSA (top), and IκBα degradation and GAPDH expression, detected by Western blotting, in the corresponding cytoplasmic extracts (bottom). The results shown are representative of at least two independent experiments.

expressed in EBV-transformed B cells (P1, P2) and SV40-transformed fibroblasts (P2) from the patients, taking seven and five control cell lines, respectively, as a reference, but not in fibroblasts bearing a large deletion in *NEMO* (Fig. 3, C and D). NEMO was barely detectable in EBV-transformed B cells and SV40-transformed fibroblasts from the patient with OL-EDA-ID. The intracellular expression of NEMO was also normal in freshly isolated monocytes and T cells from P2 (Fig. 3 E). Thus, levels of NEMO expression were strictly normal in patients bearing the E315A and R319Q mutations as shown by Western blotting and flow cytometry in hematopoietic and nonhematopoietic cell lines and in freshly prepared blood cells.

Response of blood cells and fibroblasts to LPS, R-848, TNF-α, and IL-1β

NEMO mutations in patients with EDA-ID are usually associated with impaired cellular responses to multiple stimuli, including LPS (via TLR-4), TNF-α, and IL-1β (24, 25). We thus stimulated whole blood cells from the patients and

10 healthy controls with LPS, TNF-α, IL-1β, and PMA/ionomycin, and measured the induction of IL-6 (unpublished data), IL-10, and TNF-α. The three patients displayed normal levels of IL-10 (Fig. 4 A), IL-6, and TNF-α (not depicted) production upon stimulation with LPS, IL-1β, and PMA plus ionomycin. IL-10 was also induced by TNF-α in P2 and P3, although to lower levels (Fig. 4 A). EBV-transformed B cells from P2 responded normally to R-848, an agonist of TLR-7/8, in terms of TNF-α production (Fig. 4 B). We then assessed the impact of *NEMO* mutations in fibroblasts from P2, a NEMO-deficient fibroblastic cell line bearing a large *NEMO* deletion, and fibroblasts from nine healthy controls. Fibroblasts from P2 produced normal amounts of IL-6 and IL-8 in response to both IL-1β and TNF-α (Fig. 4 C). In contrast, fibroblasts from all EDA-ID patients tested, bearing other *NEMO* mutations, showed various levels of impairment of IL-6 and IL-8 production (unpublished data). We assessed IκBα cytoplasmic degradation by Western blotting and the κB-binding activity of nuclear extracts by electrophoretic mobility shift assays. In contrast with what was observed in fibroblasts from the OL-EDA-ID patient bearing *NEMO* mutation X420W (24), both IκBα degradation and κB binding activity were completely normal in fibroblasts from P2 (Fig. 4 D). Thus, the NEMO–NF-κB signaling pathway in response to TLR4, 7, and 8 agonists, IL-1β, and TNF-α, was normal in SV40-fibroblastic and EBV-transformed B cell lines from our patients.

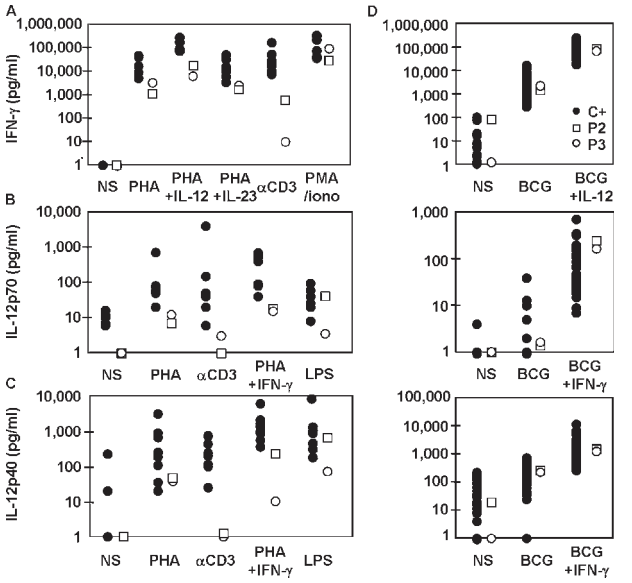

Figure 5. IL-12 and IFN-γ production by leukocytes. Cytokine production by PBMCs from 10 healthy donors, (C+, ●), P2 (□), and P3 (○) in response to PHA, alone or in combination with recombinant IL-12 (20 ng/ml), IL-23 (20 ng/ml), or IFNγ (5,000 UI/ml), anti-CD3 (10 ng/ml), LPS (1 μg/ml) and PMA/ionomycin (10^{-7}/10^{-5} M). (A) IFN-γ, (B) IL-12p70, (C) IL-12p40 production. (D) Cytokine production by whole blood cells from 50 healthy donors, P2, and P3 upon stimulation with live BCG alone or in combination with IL-12 (20 ng/ml) or IFN-γ (5,000 IU/ml): IFN-γ (top), IL-12p70 (middle), and IL-12p40 (bottom) secretion. For each patient, the results shown are representative of two independent experiments.

Impaired production of IL-12 and IFN-γ by peripheral blood mononuclear cells upon PHA activation

We previously reported that PBMCs from P1 produced small amounts of IFN-γ upon stimulation with PHA (21, 22). PBMCs from P2 and P3 produced normal amounts of IFN-γ in response to PMA/ionomycin but not in response to PHA or CD3 stimulation, with normal levels determined as those for 10 healthy controls (Fig. 5 A). In these conditions, the impaired production of IL-12 was previously shown to account for poor IFN-γ production by PBMCs in P1 (21), consistent with the poor production of IFN-γ observed in blood cells from IL-12p40- and IL-12Rβ1–deficient patients (9, 11, 33). Accordingly, PBMCs from P2 and P3 produced only small amounts of IL-12 after PHA stimulation, which were not complemented by adding IFN-γ (Fig. 5, B and C). In contrast, the addition of IL-12 partially complemented IFN-γ production (Fig. 5 A). As a control, the PHA-driven production of TNF-α and IL-10 by P2 and P3 was similar to that in 10 healthy controls (unpublished data). The production of IL-12 and IFN-γ was also normal upon stimulation with LPS and PMA/ionomycin, respectively (Fig. 5, A–C). Moreover, the production of IL-12 and IFN-γ by whole blood cells stimulated with live BCG (alone or with IFN-γ or IL-12) was normal in P2 and P3 (Fig. 5 D). Thus, the three probands displayed selective impairment of IL-12 and IFN-γ production by PBMCs upon stimulation with PHA or CD3. In contrast, the production of IL-12 was normal in response to LPS and BCG and that of IFN-γ was normal in response to PMA/ionomycin and BCG. Overall, the cellular phenotype of impaired IL-12–dependent production of IFN-γ by PHA-stimulated PBMCs is suggestive of a common pathogenic mechanism of predisposition to mycobacterial disease associated with NEMO mutations E315A and R319Q.

Impaired IL-12 secretion by PHA-stimulated monocytes and T cells

We previously described a specific defect in IL-12 production by P1 monocytes upon PHA stimulation in the presence of control T cells (21, 22). We tested cells from P2 and P3 in a similar coculture assay and measured the production of IL-12p70, IL-12p40, and IFN-γ by ELISA (Fig. 6 A). These cytokines were produced in very small amounts or not at all in monocytes stimulated with PHA in the absence of T cells or in T cells in the absence of monocytes. P2 and P3 monocytes cocultured with autologous or healthy T cells produced much less IL-12p70, IL-12p40, and IFN-γ than control monocytes cocultured with autologous, P2, or P3 T cells. The T lymphocytes of these patients produced IFN-γ after costimulation with control monocytes and PHA. The low levels of IFN-γ secretion were the result of poor IL-12 production as indicated by (a) the complementation provided by recombinant IL-12 (but not IL-23) (unpublished data) and (b) the poor production of IFN-γ documented with IL-12p40–deficient monocytes or IL-12Rβ1–deficient

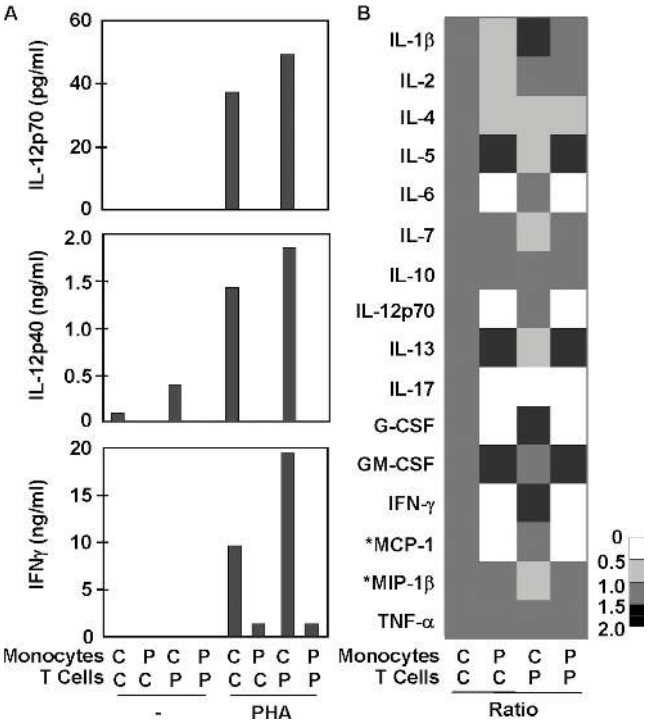

Figure 6. IL-12 and IFN-γ production by cocultured monocytes and T cells from the patients studied and healthy controls. (A) IL-12p70, IL-12p40, and IFN-γ production, measured using classical sandwich ELISA, in a mixture of purified monocytes and T cells, as indicated upon stimulation with PHA. The results shown are representative of three independent experiments for P2 and one for P3. (B) The same coculture supernatants were analyzed for a multiplex of 16 cytokines, using the Bioplex array. Each column represents the data for one monocyte–T cell coculture system, and all four columns correspond to the same experiment. Each row corresponds to one cytokine. The gray-scale bar indicates the magnitude of cytokine expression, using the control/control (C/C) coculture system as a reference. For each data point, the amount of cytokine produced in the unstimulated system was subtracted from that produced in the PHA-activated system, and the result obtained was compared with the reference value (C/C). The production of *MCP-1 and *MIP-1β by monocytes was PHA-dependent but T cell–independent, as monocytes responded to PHA by producing large amounts of these cytokines, whereas the addition of T cells did not increase cytokine production. The defects in the production of IL-6, IL-12p70, G-CSF, IFN-γ, and MCP-1 were confirmed in three independent experiments on blood cells from P2 and one experiment on blood from P3.

T cells (unpublished data). Certain monokines, such as IL-6, G-CSF, and MCP-1, were poorly induced, whereas others were induced in normal (IL-4, IL-10) or large (IL-5, IL-13) amounts by monocytes from P2 and P3, indicating that these cells were not globally unresponsive (Fig. 6 B and not depicted). Two other lymphokines (IL-2, IL-4) were not affected and the production of IL-17 was impaired. Finally, cytokines secreted by T cells and monocytes (TNF-α, IL-7, IL-10, and GM-CSF) were normally induced. All three probands had a specific immunological phenotype in which IL-12 production by monocytes in response to PHA and T cells was affected. Impaired IFN-γ production does not reflect an intrinsic T cell defect and is instead a consequence of impaired IL-12 production by monocytes.

PHA-activated T cell–dependent monocyte secretion of IL-12 is driven by CD40

The two *NEMO* mutations exerted their effects downstream from monocyte receptors triggering the induction of IL-12. The CD40 signaling pathway has been shown to be critical for the T cell–dependent induction of IL-12 in monocytes and dendritic cells (34–37). After PHA stimulation, PBMCs from CD40- and CD40L-deficient patients (38) produced much lower levels of IL-12 and IFN-γ than did PBMCs from 10 healthy controls (unpublished data), consistent with previous data (39). The induction of IL-12 by LPS and that of IFN-γ by PMA/ionomycin were normal (unpublished data). IL-12 induction was abolished if CD40L-deficient T cells were cocultured with healthy or CD40L-deficient monocytes, resulting in low levels but not the total absence of IFN-γ production (Fig. 7 A). Conversely, normal IL-12 induction was observed if control or CD40L-deficient monocytes were mixed with T lymphocytes from a healthy donor. Low levels of IFN-γ induction were associated with the presence of small amounts of IL-12 in this assay. IL-12 induction was abolished if CD40-deficient monocytes were incubated with CD40-deficient or normal T cells (Fig. 7 B). Paradoxically, IFN-γ secretion was not significantly impaired, perhaps reflecting the direct cross-linking of CD40L by PHA (40). In contrast, control monocytes produced normal amounts of IL-12 when cultured with control or CD40-deficient T cells. Our findings for the monocyte–T cell coculture assay unambiguously indicate that the engagement of the monocyte CD40 by CD40L-expressing T cells is required for the optimal induction of IL-12 production. These data suggest that the *NEMO* mutations in P1, P2, and P3 were pathogenic as a result of their impact on CD40 signaling within monocytes, leading to low levels of IL-12 secretion upon T cell stimulation.

NEMO mutation impairs CD40 signaling in dendritic cells but not B cells

We assessed the responses to CD40 stimulation of cells from our patients. We first incubated purified monocytes from P2 with mouse fibroblastic L cells (L-cells) and L-cells stably transfected with a construct encoding human CD40L (L-cells-hCD40L). Monocytes from P2 did not produce IL-12, IL-6, and TNF-α upon stimulation with L-cells-hCD40L (unpublished data). We then tested monocyte-derived dendritic cells (MDDCs) as DCs are major producers of IL-12 in vivo. MDDCs produce large amounts of IL-12 upon CD40 stimulation in vitro (36). MDDCs from P2 and P3 were activated with LPS plus IL-1β, L-cells, or L-cells-hCD40L with or without IL-1β. MDDCs from P2 and P3 displayed severely impaired cytokine production in response to L-cells–hCD40L but not in response to LPS plus IL-1β (Fig. 7 C), whereas induction of the costimulatory molecules

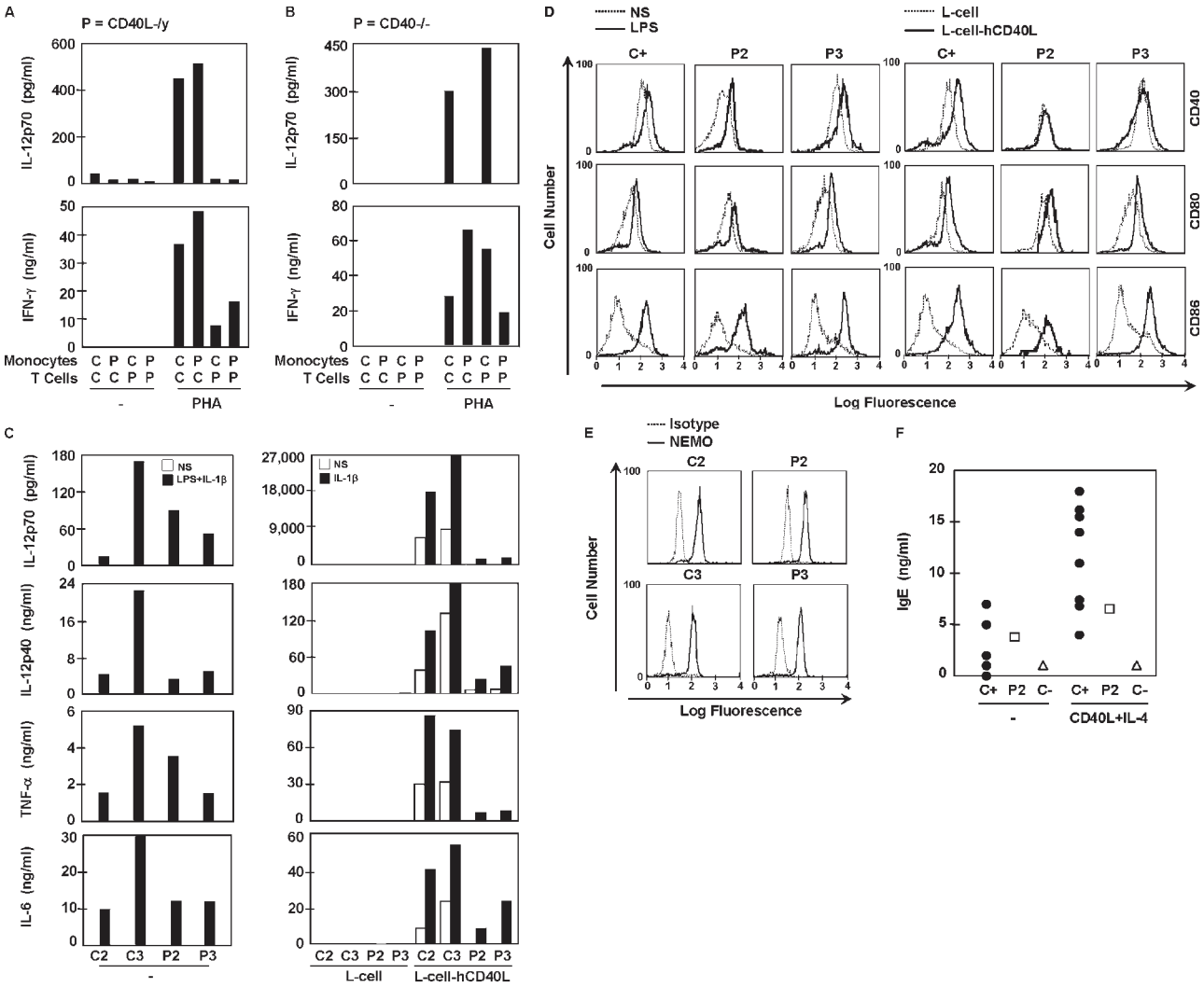

Figure 7. The impact of CD40 and CD40L deficiency on IL-12 and IFN-γ production. IL-12p70, IL-12p40, and IFN-γ production, measured by classical sandwich ELISA, in a mixture of purified monocytes and T cells, as indicated, upon stimulation with PHA from a healthy donor with (A) CD40L- and (B) CD40-deficient PBMCs. MDDCs obtained from two healthy controls (C2 and C3), P2 and P3, after 24 h of incubation alone or with LPS (1 μg/ml) plus IL-1β (10 ng/ml) as a control of CD40-independent activation, cocultured with L-cells transfected with human CD40L (L-cell-hCD40L) and nontransfected L-cells (L-cell): (C) IL-12p70, IL-12p40, TNF-α, and IL-6 production, measured by classical sandwich ELISA, and (D) FACS analysis of cell surface expression of CD40, CD80, and CD86 costimulatory molecules gating on CD1a-positive MDDCs. (E) Intracellular staining of NEMO protein in MDDCs from P2 and P3, and their respective controls (C2 and C3) in the experimental conditions of Fig. 3. (F) IgE secretion by B cells in vitro, as measured by ELISA, after the activation of PBMCs from 20 healthy controls (C+, ●), P2 (□), and a CD40-deficient patient as the negative control (C−,△), with soluble CD40L in combination with IL-4. The results shown are representative of two independent experiments.

CD80 and CD86, unlike that of CD40, was maintained (Fig. 7 D). These data are consistent with our previous observations in a child with a severe *NEMO* mutation associated with OL-EDA-ID and severe mycobacterial infection (24). MDDCs from P2 and P3 expressed normal levels of NEMO (Fig. 7 E). B cells from P2 produced normal amounts of IgE in response to costimulation with IL-4 and CD40L, as shown by ELISA, with data from 20 healthy controls and a CD40-deficient patient used as a reference (Fig. 7 F). Moreover, B cell proliferation, as assessed by the measurement of [^{3}H] thymidine incorporation, was also normal (unpublished data). These data suggest that the CD40 signaling pathway was not affected in B cells in vitro, consistent with the normal B cell switch and antibody response in vivo in our patients. Altogether, these findings suggest that the patients with XR-MSMD bearing the E315A and R319Q mutations in NEMO suffered from mycobacterial disease as a result of the impaired IL-12 production by monocytes and dendritic cells after stimulation with the CD40L on T cells.

Delayed nuclear accumulation of NF-κB/c-Rel in CD40-stimulated dendritic cells

We evaluated the impact of the *NEMO* mutations identified by confocal microscopy analysis of the subcellular distributions

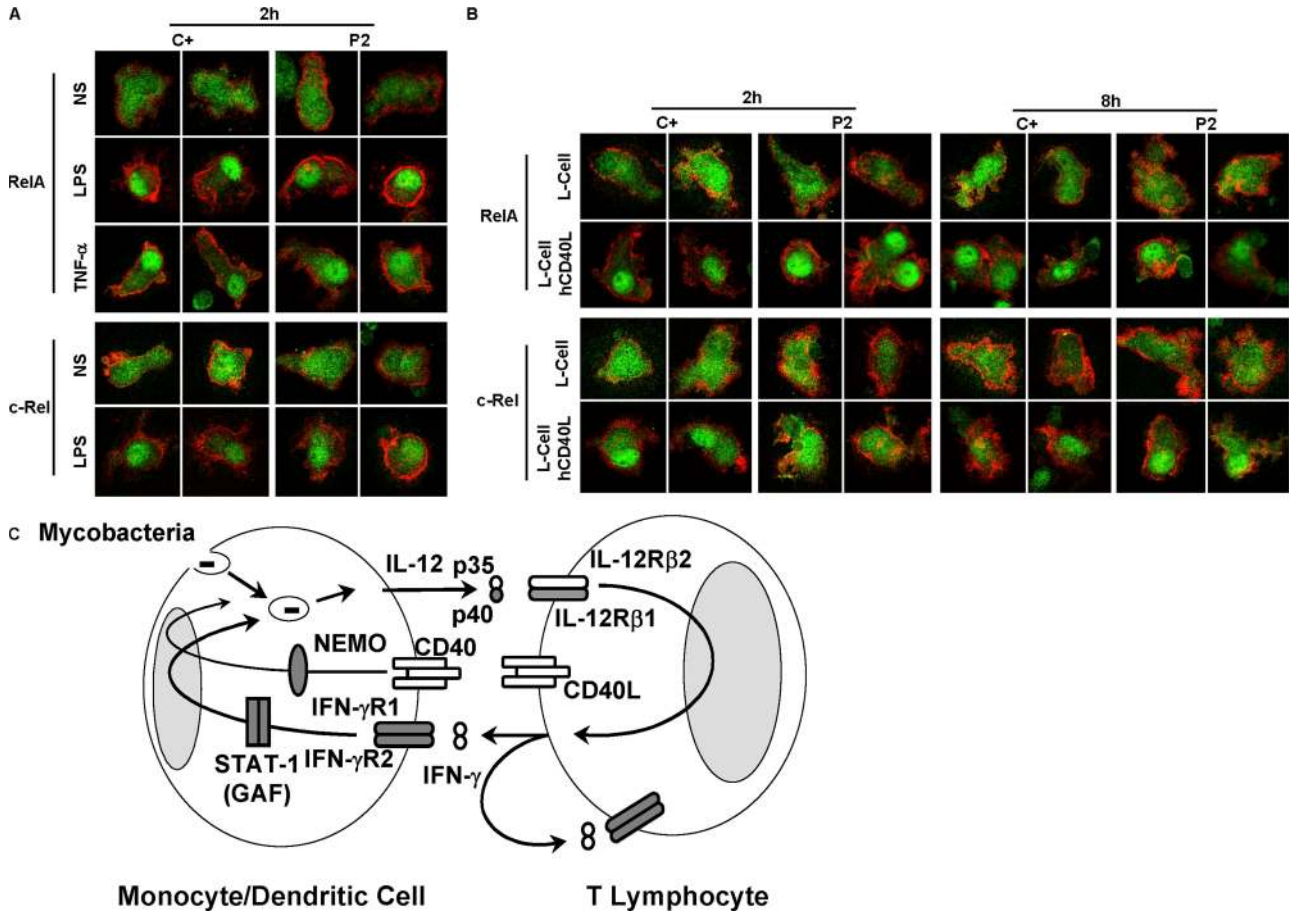

Figure 8. Endogenous RelA/p65 and c-Rel localization in MDDCs upon CD40L stimulation. Isolated monocytes from a healthy control (C+) and P2 were cultured for 8 d with GM-CSF and IL-4 to generate MDDCs. MDDCs were serum starved for 20 h before activation. MDDCs were incubated alone or activated with (A) LPS (1 μg/ml), TNF-α (20 ng/ml), and (B) cocultured with L-cells transfected with human CD40L (L-cell-hCD40L) or nontransfected L-cell line (L-cell) and fixed by incubation in 4% PFA. MDDCs were surface stained with mouse anti–human CD1a and Cy3-conjugated goat anti–mouse IgG (red) and endogenous RelA and c-Rel were stained with Alexa-488–conjugated goat anti–rabbit IgG against primary rabbit antibody (green). The nucleus was stained with DAPI (not depicted). (C) Schematic representation of cytokine production and cooperation between monocytes/dendritic cells and T cells. The IL-12/IFN-γ loop and the CD40L-activated CD40 pathway, mediating cooperation between T cells and monocyte/dendritic cells, are crucial for protective immunity to mycobacterial infection in humans. IL-12 production is controlled by both IFN-γ and CD40-NEMO-NF-κB signaling. Mutant molecules in patients with MSMD are indicated in gray. Allelic heterogeneity of the five autosomal disease-causing genes results in the definition of 12 genetic disorders. The *NEMO* mutations in the LZ domain mostly impair CD40-NEMO-dependent pathways and define the X-linked form of MSMD.

of the NF-κB subunits RelA (p65) and c-Rel in MDDCs from P2 and a healthy control, unstimulated and in response to LPS, IL-1β, TNF-α, mouse L-cells, or human CD40L-expressing mouse L-cells. LPS treatment resulted in the nuclear accumulation of RelA and c-Rel in MDDCs from both the healthy control and P2 (Fig. 8 A). IL-1β induced the translocation of RelA, but not of c-Rel, in MDDCs from both the healthy donor and P2 (unpublished data). The nuclear translocation of RelA in response to TNF-α seemed to be less efficient in MDDCs from P2 (Fig. 8 A), possibly accounting for the weak induction of IL-10 in PBMCs (Fig. 4 A). The translocation of RelA in response to CD40 stimulation was normal in MDDCs from P2 up to 8 h after stimulation (Fig. 8 B). In contrast, the nuclear accumulation of c-Rel in response to CD40 was clearly impaired in MDDCs from P2, 2 (Fig. 8 B) and 5 h after stimulation (not depicted). Only after 8 h of stimulation was c-Rel accumulation detected in the nuclei of MDDCs from P2 (Fig. 8 B). These data strongly suggest that the *NEMO* mutation identified in P2 impairs CD40-triggered NF-κB activation by delaying the nuclear accumulation of c-Rel. They also suggest that CD40-driven, NEMO-dependent IL-12 production in human MDDCs depends on c-Rel, as previously shown in mice (41, 42). Furthermore, our data indicate that the R319Q and E315A mutations in the NEMO LZ domain are associated with XR-MSMD because they impair the T cell–dependent, CD40-triggered, NF-κB/c-Rel–mediated induction of IL-12 in monocytes and dendritic cells (Fig. 8 C).

DISCUSSION

We describe here the first genetic etiology of XR-MSMD, a syndrome clinically defined for the first time in 1994 in a multiplex American kindred (1, 21), after the publication of individual case reports (20). The four patients from this family carried the E315A mutation in NEMO. XR-MSMD is not limited to a single family, as a different, but related NEMO mutation, R319Q, was found in two unrelated European boys, from France and Germany. *NEMO* is the sixth MSMD-causing gene to be identified, after the identification of *IFNGR1* in 1996 (6, 7), *IFNGR2*, *IL12B,* and *IL12RB1* in 1998 (8–11), and *STAT1* in 2001 (18) (Fig. 8 C). It is the sixth genetic defect associated with MSMD but the 13th genetic etiology of this syndrome, given the considerable allelic heterogeneity of previously reported defects of the IL-12–IFN-γ circuit (15) (unpublished data). One of our patients with EM disease (II.4 in kindred A) also suffered from miliary tuberculosis in childhood, and two of our probands (P2 and P3) probably suffered from tuberculosis, as the sole infectious phenotype suggested by consistent histological results and strongly positive tuberculin skin tests. Patients with BCG and EM diseases and otherwise healthy children with severe tuberculosis should therefore be investigated for *NEMO* mutations (5). The possibility of *NEMO* mutations cannot be excluded by the absence of developmental signs, as shown in four of our six patients and in two other recently reported patients (43).

We can now suggest a rationale for the pathogenesis of mycobacterial diseases in patients with XR-MSMD. The two causal *NEMO* mutations impair CD40 signaling in monocytes and dendritic cells, delaying the nuclear accumulation of NF-κB/c-Rel and impairing IL-12 secretion upon stimulation by CD40L-expressing T cells. In turn, impaired IL-12 production by antigen-presenting cells results in impaired IFN-γ production by T cells. X-linked *NEMO* is thus physiologically connected to the five autosomal IL-12/23–IFN-γ circuit genes known to cause MSMD (4). These data are consistent with the observation that CD40-deficient (44) and CD40L-depleted mice (45) are susceptible to *Mycobacterium avium* infections. CD40L-deficient mice are also susceptible to BCG and CD40-deficient mice are susceptible to *Mycobacterium tuberculosis* (46, 47). Moreover, CD40L-deficient patients frequently develop localized disease caused by BCG, and severe tuberculosis (5, 48). However, human *CD40* and *CD40L* are not recognized as bona fide MSMD-causing genes, as CD40- and CD40L-deficient patients have never been reported to suffer from disseminated BCG or EM disease. This implies that pathways other than CD40–NEMO–IL-12, such as the TNF-α signaling pathway (Figs. 4 A and 8 A) (49), are probably involved in the pathogenesis of diseases caused by EM, at least, in patients with mutations in the *NEMO* LZ domain. In any event, human phagocytes and dendritic cells require T cell stimulation via CD40, NEMO, and c-Rel to produce the amounts of IL-12 necessary to control mycobacteria in natural conditions of infection (50).

Null mutations in *NEMO* are lethal in utero in male fetuses (27). Patients with hypomorphic mutations in *NEMO* suffer from XR-EDA-ID (23–26). To date, 36 patients bearing 28 different *NEMO* mutations have been described (23–27, 32, 43, 51–55) (unpublished data). 11 out of the known 36 XR-EDA-ID patients have developed severe mycobacterial infection, mostly caused by *M. avium*. However, these patients also suffered from infections caused by many other microorganisms. In contrast, five of our six patients presented mycobacterial disease as their sole invasive infection. The invasive *Haemophilus influenzae b* infection in one of our patients may not have occurred by chance. Similarly, two out of the six patients had conical incisors (decidual teeth in one and permanent teeth in the other), implying that the penetrance of these particular NEMO genotypes was low (but not null) for pyogenic infections and developmental defects, but high for mycobacterial disease. Our report stresses the heterogeneity of phenotypes associated with hypomorphic *NEMO* mutations. Two patients with XR-EDA-ID, both with the X420W genotype, presented XR-OL-EDA-ID (24, 53, 54). Most patients present the less severe clinical syndrome of XR-EDA-ID, with typical (23–25) or hidden (conical incisors) (26) developmental signs and multiple infections. Two other patients with severe infections but no developmental disorder were recently reported (43). Finally, we report here two novel *NEMO* mutations, responsible for MSMD in six patients. All six patients are selectively susceptible to mycobacteria and display selective impairment of the CD40-dependent induction of IL-12 in antigen-presenting cells. These findings provide the first link between a *NEMO* genotype and immunological and infectious phenotypes.

Why do these two mutations have selective effects? The E315A and R319Q mutations are located in the LZ domain of NEMO and do not affect protein expression. Residues E315 and R319 probably form a salt bridge that is disrupted by the two pathogenic mutations (Fig. 2 C). The two mutations may induce local plasticity in a region of the LZ domain critical for signaling via CD40, but less important for other signaling pathways. However, CD40 signaling was not totally abolished in dendritic cells from our patients, as the nuclear accumulation of RelA, and the induction of CD80 and CD86 were normal, whereas the induction of CD40 was not. These findings are consistent with the normal CD40-mediated induction of HLA-II and CD86 previously reported in dendritic cells from a patient with OL-EDA-ID (24). It is unknown whether the CD40–CD80/86 and CD40–HLA-II pathways are truly NEMO independent or whether they are unaffected by the NEMO mutations tested. The E315A and R319Q NEMO mutations impair at least one CD40 signaling pathway involving NF-κB–c-Rel in monocytes and dendritic cells, but they have no significant effect on B cells, in vivo and in vitro, unlike other previously reported *NEMO* mutations (24, 25, 52, 55). In conclusion, specific *NEMO* mutations may selectively target the CD40–NF-κB–c-Rel signaling pathway in monocytes and dendritic

cells, preventing the production of sufficient quantities of IL-12 after T cell stimulation. This results in impaired IFN-γ–mediated immunity and predisposition to mycobacterial diseases (Fig. 8 C).

MATERIALS AND METHODS

Case reports. The first family (kindred A) with XR-MSMD has been described elsewhere (1, 20–22). None of the family members were vaccinated with BCG. Severe *M. avium* infection was documented in four maternally related male family members in two successive generations (Fig. 1 A; patients II.1, II.4, III.7, and III.8). The clinical features of patient 1 (P1, II.4), the index case, have been described elsewhere (1, 20). In brief, at the age of 13 yr, P1 presented granulomatous cutaneous lesions, thought to be sarcoid. Extensive erosive lesions on the face and arm were subsequently found to be the result of *M. avium* complex infection. Treatment with rifampicin, ethambutol, clofazimine, isoniazid and streptomycin was initiated. After 2.5 yr of therapy, smears and cultures of skin from the patient's face and arm remained positive for *M. avium* complex X cluster. Intensive antibiotic and IFN-γ therapy has led to periods in which the skin has healed and cultures have tested negative, but this patient has frequently displayed intermittent mycobacteremia over the last 10 yr. Three other family members also developed disseminated *M. avium* complex infection. Patient II.1 was cured of miliary tuberculosis at the age of 6 yr. Disseminated *M. avium* infection occurred in this patient at the age of 40 yr, and was never completely eradicated. The patient died of *Enterobacter* bacteremia complicating parenteral nutrition at the age of 48 yr. Patient III.7 was successfully treated for disseminated *M. avium* infection at the age of 5 yr, but died in an automobile accident at the age of 10. His brother, patient III.8, had recurrent *Haemophilus influenzae* bacteremia at the age of 6 yr. At the age of 14 yr, he presented disseminated *M. avium* complex infection involving abdominal lymph nodes and blood. Overt signs of ectodermal dysplasia (conical teeth, hypodontia, hypotrichosis, abnormal hair whorl) were evaluated. This patient has remained mycobacteremic despite treatment with multiple antibiotics and IFN-γ. Sparse teeth were the only developmental abnormality on physical examination, and long went unrecognized in patient 1 (Fig. 1 B, left). Cells of the various blood lineages and lymphoid subsets (CD3, CD4, CD8, CD20, CD16, CD56) were present in normal numbers. T cells proliferated normally in vitro in response to mitogenic (PHA) and antigenic (recall antigens) stimulation. In P1, serum levels of Ig isotypes (IgG, IgM, IgA, IgE, IgD) were normal for age, and there was a normal Ab response to protein and polysaccharide antigens.

The second family (kindred B) included a single patient (P2, II.1), an 8-yr-old boy, born to unrelated parents of Italian and Serbian descent living in France (Fig. 1 A). At the age of 2 mo, this child was vaccinated with BCG. At the age of 2 yr, he was hospitalized for persistent low-grade fever (38°C) with night sweats, cough, and cervical and inguinal lymphadenopathy. Serum C-reactive protein (CRP) levels (31 mg/l) and erythrocyte sedimentation rate (ESR) were high (32 mm/h), as was leukocyte count, at 15,200 leucocytes/mm^3. Chest X-ray and pulmonary function tests were normal. Urine, gastric, and blood cultures for mycobacteria were negative, but the patient had a strongly positive tuberculin skin test (TST) (24-mm induration). The patient was treated with isoniazid and rifampicin for 6 mo, and his condition improved. Approximately 1 yr after the end of treatment, he was hospitalized for cervical lymphadenitis and prolonged fever. The TST was again positive (10 mm). Four lymph nodes were excised and a biopsy revealed granulomas with no visible acid-fast bacilli. Cultures were negative. The patient also had diarrhea, with *Salmonella enteritidis* identified in the stools, from which he recovered spontaneously. He is now 8 yr old and clinically well with no treatment. Conical decidual incisors were the only developmental abnormality on physical examination, and this abnormality was long unrecognized (Fig. 1 B, middle). Permanent teeth were normal in shape and number, as shown by clinical examination and mandibular X ray (unpublished data). Cells of the various blood lineages and lymphoid subsets (CD3, CD4, CD8, CD19, CD16, CD56) were present in normal numbers. T cells proliferated normally in vitro in response to mitogenic (PHA) and antigenic (recall antigens) stimulation. The NBT assay and chemioluminescence of PMNs were normal. Serum levels of Ig isotypes (IgG, IgM, IgA, IgE, IgD) were normal for age, and there was a normal Ab response to protein antigens. Serum titers of allo-hemagglutinins were normal (group B). The patient had no detectable antibodies against polysaccharide antigens at the age of 6 yr, when he was immunized with 23-valent nonconjugated pneumococcal vaccine, but mounted a normal response at the age of 7 yr, after two injections of nonconjugated pneumococcal vaccines.

The third family (kindred C) included a single patient (P3, II.1), an 11-yr-old boy, born to unrelated German parents living in Germany (Fig. 1 A). He was not vaccinated with BCG. At the age of 1 yr, he was hospitalized for a cervical abscess caused by *Haemophilus influenzae b*, which responded well to surgery and antibiotic treatment. At 9 yr of age, he was hospitalized for persistent low-grade fever (38°C) of unknown origin. He presented splenomegaly, marked hypergammaglobulinemia, and granulocytopenia. After his discharge from the hospital, he suffered recurrent infections, including bronchitis and pneumonitis. At the age of 10 yr and 4 mo, he had a strongly positive TST (20-mm induration), whereas negative results had been obtained for this test on three previous occasions, at the ages of 7, 8, and 9 yr. At the same time, an ELISPOT assay for IFN-γ after ESAT-6 stimulation was negative. Chest X-ray showed no mediastinal lymph node enlargment, but did show infiltration of the lower parts of both lungs. A tentative diagnosis of mycobacterial disease was made, and the patient was treated with isoniazid for 3 mo. This treatment was stopped as it seemed to cause headaches, but the patient was subsequently treated with cefpodoxime prophylaxis. No developmental abnormalities, not even conical teeth, were observed on physical examination (Fig. 1 B, right). Mandibular X-ray indicated an absence of hypodontia. Cells of the various blood lineages and lymphoid subsets (CD3, CD4, CD8, CD19, CD16, CD56) were present in normal numbers. T cells proliferated normally in vitro in response to mitogenic (PHA) and antigenic (recall antigens) stimulation. The results of NBT and dihydrorhodamine tests were normal. Serum levels of the immunoglobulin IgG, IgM, and IgD isotypes were high (maximum titers: IgG 70.85 g/liter, IgM 1.54 g/liter, and IgD 304 IU/ml). Serum IgA and IgE levels were normal. There was a normal Ab response to protein antigens. There were no allo-hemagglutinins (group A). The patient had detectable, but very low titers of antibodies against polysaccharide antigens at the age of 11 yr, before vaccination. After vaccination with 23-valent nonconjugated vaccine at the age of 11 yr, titers rose and reached normal levels.

Mutations in the five known MSMD-causing autosomal genes (*IFNGR1*, *IFNGR2*, *STAT1*, *IL12B*, *IL12RB1*) were excluded in the three kindreds by means of genetic and immunological assays (unpublished data). Other patients with well-defined genetic defects were enrolled in our study, including patients with IL-12p40 deficiency, IL-12Rβ1 deficiency, IFN-γR1 deficiency, CD40 deficiency, and CD40L deficiency. Their genetic lesions are available upon request. Our study was conducted according to the principles expressed in the Helsinki Declaration and was approved by our Institution Review Boards. An informed consent was provided by all patients studied, or by their parents, in the case of children.

Blood cell culture and stimulation. Whole blood samples were diluted 1/2 in RPMI 1640 (GIBCO BRL) and infected by incubation with live *M. bovis* BCG (Pasteur substrain), at a multiplicity of infection of 20:1, alone or with recombinant IFN-γ (5,000 IU/ml; Imukin, Boehringer Ingelheim) or recombinant IL-12p70 (20 ng/ml; R&D Systems), LPS (from *Salmonella minnesota*, 1 μg/ml; Sigma-Aldrich), TNF-α (20 ng/ml; R&D Systems), IL-1β (10 ng/ml; R&D Systems), phorbol 12-myristate 13-acetate (PMA) (10^{-7} M; Sigma-Aldrich) with ionomycin (10^{-5} M; Sigma-Aldrich) and supernatants were recovered after 14 and 48 h. Cytokine production was normalized according to the number of PBMCs in the individual tested. PBMCs were obtained from patients and healthy donors by centrifuging heparin-treated blood diluted 1/2 in RPMI 1640 on Ficoll-Paque Plus (GE Healthcare), followed by isolation in mononuclear cell medium. PBMCs were cultured in

RPMI 1640 medium (GIBCO BRL) supplemented with 10% heat-inactivated pooled FBS (GIBCO BRL), referred to as complete RPMI 1640. Cells (10^6 PBMCs/ml/well) were activated by incubation with phytohemagglutinin-P 1/700 (PHA, Bacto PHA-P; Becton Dickinson), alone or in combination with recombinant IFN-γ (5,000 IU/ml; Imukin, Boehringer Ingelheim) or recombinant IL-12p70 (20 ng/ml; R&D System) or IL-23 (20 ng/ml; R&D Systems), anti-CD3 antibody (10 ng/ml, OKT3, OrthoPharmaceutical) and LPS (from *Salmonella minnesota*, 1 μg/ml; Sigma-Aldrich) for 14 and 48 h.

Culture and stimulation of cell lines. Fibroblast cell lines were derived from dermal biopsy samples from patients and healthy donors and immortalized by transformation with a plasmid-containing SV40 large T antigen. We added 10^5 fibroblasts to DMEM (GIBCO BRL) supplemented with 10% (vol/vol) heat-inactivated FBS (GIBCO BRL) in each well of a 24-well plate. Fibroblasts were stimulated with TNF-α (20 ng/ml; R&D Systems), IL-1β (10 ng/ml; R&D Systems), or PMA (10^{-7} M; Sigma-Aldrich) plus ionomycin (10^{-5} M; Sigma-Aldrich) and supernatants were recovered after 24 h of activation. B lymphocytes were immortalized with Epstein-Barr virus (EBV-transformed B cells) and cultured in complete RPMI 1640. EBV-transformed B cells were stimulated with imidazoquinolone R-848, an agonist of TLR-7 and TLR-8 (provided by R. Miller, 3M Pharmaceuticals and 3M Innovative Properties Company, St. Paul, MN) for 24 h.

Genetic analysis. Genomic DNA was isolated by phenol/chloroform extraction from blood cells, which were washed in TE 10:1 buffer (10 mM Tris, 1 mM EDTA, pH 7.6) and lysed in extraction buffer (10 mM Tris, 0.1 M EDTA, 0.5% SDS, and 10 mg/ml proteinase K) overnight at 37°C. RNA was extracted from EBV-transformed B cell lines or SV40-transformed fibroblasts with TRIzol (Invitrogen), according to the kit manufacturer's instructions. We used 1–5 μg total RNA for direct reverse transcription with Oligo-dT (Invitrogen). PCR was performed using *Taq* polymerase (Invitrogen), and the GeneAmp PCR System 9700 (Applied Biosystems). Primer sequences for the amplification of *NEMO* exons and cDNA are available upon request. PCR products were purified by centrifugation through Sephadex G-50 Superfine resin (GE Healthcare) and sequenced with the BigDye Terminator Cycle sequencing kit (Applied Biosystems). Sequencing products were purified on Sephadex G-50 Superfine resin and sequences were analyzed on a 3100 ABI Prism Genetic Analizer (Applied Biosystems).

Western blot and EMSA. For EMSAs, nuclear extracts were prepared from SV40-transformed fibroblasts, after incubation with or without IL-1β (10 ng/ml) and TNF-α (20 ng/ml) for 20, 40, and 60 min. We used the Bio-Rad Laboratories protein assay to adjust protein concentrations such that all samples contained similar amounts of protein. EMSA was performed with a [^{32}P]-labeled NF-κB–specific DNA probe (5′-GATCATGGGGAATCCCCA-3′, 5′-GATCTGGGGAATTCCCCCAT-3′). For Western blotting, total protein was extracted from SV40-transformed fibroblasts and EBV-transformed B cells. Cytosolic extracts were prepared from SV-40–transformed fibroblasts with or without stimulation with IL-1β (10 ng/ml) and TNF-α (20 ng/ml). Protein fractions were separated by reducing SDS-PAGE and electrotransfered onto nitrocellulose membranes (Schleicher & Schuell). Membranes were blocked by incubation in 5% nonfat milk powder (Nestle USA) in 0.05% Tween-20 in PBS for 60 min at room temperature. NEMO was detected using rabbit polyclonal anti-NEMO antibodies (3328 and p18, gifts from G. Courtois, INSERM, Saint Louis Hospital, Paris, France), rabbit antibodies against GAPDH (SC-25778, Santa Cruz Biotechnology, Inc.), rabbit anti-IκBα (C-21, sc-37, Santa Cruz Biotechnology, Inc.), and mouse antibodies against Stat-3 (Santa Cruz Biotechnology, Inc.). Membranes were washed several times in 0.05% Tween-20 in PBS, and antibody binding was detected by incubation with horseradish peroxidase–conjugated anti–rabbit secondary antibodies (GE Healthcare), using the ECL system (GE Healthcare).

Purification of peripheral T cells and monocytes. For T cell isolation, we depleted peripheral PBMCs of adherent cells and performed negative immunomagnetic depletion using a cocktail of antibodies against CD14, CD16, CD19, CD36, CD56, CD123, and glycophorin A (Macs; Miltenyi Biotec), according to the kit manufacturer's instructions. The preparation was >95% pure, as assessed by flow cytometry with FITC-CD2 and PE-CD3 staining (BD Biosciences). Monocytes were isolated from peripheral PBMCs by negative immunomagnetic depletion, using a cocktail of antibodies against CD3, CD7, CD16, CD19, CD56, CD123, and glycophorin A (Macs; Miltenyi Biotec), according to the kit manufacturer's instructions. Monocytes were >80% pure, as assessed by flow cytometry with PE-CD14 (BD Biosciences) staining.

Coculture of monocytes and T cells. We plated 10^5 monocytes per well in complete RPMI 1640 medium in 24-well plates (Nunc) and incubated them for 3 h at 37°C in an atmosphere containing 5% CO_2. The nonadherent cells were washed off and the adherent cells were incubated overnight with 400 μl of complete RPMI 1640. The following day, T cells were purified as described in a previous paragraph and 5×10^5 T cells were added to the monocytes. Selected wells were stimulated with a 1/700 dilution of PHA (Bacto PHA-P; Becton Dickinson), alone or in combination with recombinant IFN-γ (5,000 IU/ml; Imukin, Boehringer Ingelheim, France), recombinant IL-12p70 (20 ng/ml; R&D Systems), and recombinant IL-23 (20 ng/ml; R&D Systems). Supernatants were collected 14 and 48 h after activation.

Generation of dendritic cells from purified monocytes. MDDCs were obtained from purified monocytes as described in a previous paragraph. They were incubated for 2 h in complete RPMI 1640 medium at 37°C under an atmosphere containing 5% CO_2 to remove all nonadherent cells, thereby increasing purity. The adherent cells were cultured in complete RPMI 1640 in the presence of GM-CSF (50 ng/ml; R&D Systems) and IL-4 (10 ng/ml; R&D Systems). Optimal conditions were maintained by splitting these cultures every 2 d. Cells were collected on day 7, when the cultures contained >95% immature $CD1a^+$ (BD Biosciences) dendritic cells.

CD40 activation. Mouse fibroblastic L-cells transfected with the human ligand of CD40 (L-cell-hCD40L) were used to induce CD40 activation on MDDCs. Nontransfected L-cells were used for control cultures. L-cells were first treated with 10 μg/ml mitomycin (Sigma-Aldrich) in sterile 1 x PBS for 2 h at 37°C in 5% CO_2. L-cells were washed five to seven times in 1 x PBS to remove all trace of mitomycin. We then plated 10^4 L-cells per well in 24-well plates and incubated them for 2 d in complete RPMI 1640 at 37°C in an atmosphere containing 5% CO_2. We incubated 2×10^5 MDDCs in complete RPMI 1640 with mitomycin-treated L-cells and recovered cell-free supernatants for cytokine analysis and MDDCs for cell surface phenotyping of CD40, CD80, and CD86 (BD Biosciences) by flow cytometry 24 h later. CD40 was activated on B cells with a mixture of soluble recombinant CD40L (500 ng/ml; Amgen) and IL-4 (100 IU/ml; R&D Systems). In brief, PBMCs were cultured for 5 d for proliferation (assessed by [^{3}H]thymidine incorporation) assays and 12 d for the measurement of IgE production (assessed by ELISA) as previously described (43).

Flow cytometry. For the staining of NEMO in EBV-transformed B cells, fibroblastic cell lines, and highly purified monocytes and T cells isolated from PBMCs, we fixed 2×10^5 cells with 4% paraformaldehyde (PFA, Fluka) in 1 x PBS and permeabilized the cells by incubation in 0.1% saponin (Sigma-Aldrich) in PBS. The cells were incubated with anti-NEMO (611306; BD Biosciences) antibody and the corresponding mouse IgG1 isotype (BD Biosciences), and primary antibody binding was detected by incubation with Alexa Fluor 488–labeled anti–mouse antibodies (Invitrogen). Cell surface phenotyping was performed by flow cytometry, in MDDCs incubated with L-cell or L-cell-hCD40L, using directly labeled antibodies. Dual-color fluorescence assays were performed with PE-CD1a

(BD Biosciences) in combination with FITC-CD40, FITC-CD80, and FITC-CD86 (all from BD Biosciences). The respective isotype controls were performed with mouse PE-IgG_{2k} (BD Biosciences) and mouse FITC-IgG_{1k} (BD Biosciences). Fluorescence was analyzed with a FACScan apparatus (Becton Dickinson), using CELLQuest software.

Cytokine analysis. Cytokine concentrations in supernatants were measured by two-sided sandwich ELISA, according to the kit manufacturer's instructions: IL-12p40, IL-12p70, G-CSF (R&D Systems), and TNF-α, IFN-γ, IL-10, IL-6, IL-8 (Sanquin). Multiplex cytokine assays were also performed on culture supernatants, using a cocktail of 17 cytokines: IL-1β, IL-2, IL-4, IL-5, IL-6, IL-7, IL-8, IL-10, IL-12p70, IL-13, IL-17, TNF-α, IFN-γ, GM-CSF, G-CSF, MCP-1, and MIP-1β (Bio-Plex Suspension Array System).

Structural modeling of the NEMO oligomerization domain. The NEMO sequence encompassing the CC2-LZ region is not >30% of identity to any reference protein in the Protein Data Bank. We therefore used experimental data to search for compatible structure references. The NEMO oligomerization domain forms a globular trimer by equilibrium sedimentation with a hydrodynamic radius of 26.1 Å, as shown by gel filtration (30) and dynamic light scattering (unpublished data), and the CC2 and LZ coiled-coil subdomains interact by fluorescence polarization (30). Limited proteolysis in combination with mass spectrometry identified a trypsin-sensitive site at residue Lys302, coinciding with the loop connecting the CC2 and LZ coiled-coils (unpublished data). Finally, the CD spectrum of the trimer showed it to contain 92% α-helix at 277 K (unpublished data). Based on these data, we used the HIV-1 gp41 ectodomain (PDB no. 1F23; reference 31) as a structure reference to provide atomic coordinates. The trimeric CC2-LZ domain of NEMO was modeled using the Insight II program (Accelrys, Inc.). The model was constructed by manually docking the Cα backbone of the CC2 coiled-coil (residues 260–292) with that of the LZ coiled-coil (residues 306–344) in an antiparallel manner. During docking, we looked for unfavorable and favorable contacts between the CC2 and LZ atoms, by calculating electrostatic and van der Waals interaction energies, using the Docking module of Insight II. The resulting energy-minimized model is shown in Fig. 2.

Immunoflurescence microscopy. MDDCs were allowed to differentiate and were activated by CD40L-expressing fibroblasts, as previously described. MDDCs were immediately fixed upon activation, by incubation in 4% formaldehyde/PBS at 4°C for 20 min, followed by surface staining with mouse anti–huamn CD1a (BD Biosciences) at 4°C for 15 min. Cells were washed in PBS and incubated with goat Cy3-conjugated anti–mouse IgG antibody (Zymed Laboratories). For intracellular staining, MDDCs were permeabilized by incubation in 0.2% Triton X-100 (Sigma-Aldrich) in PBS for 15 min. Cells were washed twice in PBS, blocked by incubation with FcR-blocking reagent (Macs; Miltenyi Biotec) for 20 min and washed once with PBS. MDDCs were incubated with 1 μg primary antibody/PBS, rabbit anti-p65 (C20, Santa Cruz Biotechnology, Inc.) and rabbit anti–c-Rel (C; Santa Cruz Biotechnology, Inc.) at 4°C for 30 min and were washed with PBS. Cells were incubated with Alexa 488–conjugated goat anti–rabbit IgG antibody (1:300 dilution) (Invitrogen) and with 4,6-diamidino-2-phenylindole (DAPI) (1/10,000 dilution; Invitrogen) for 15 min. They were washed at least three times with PBS. MDDCs were resuspended in 100 μl of PBS and plated on lysine-coated slides (VWR), using the Cytospin system. The coverslips were mounted on glass slides with Mowiol. Slides were viewed under an LSM 510 confocal microscope.

We thank A. Munnich, A. Smahi, C. Hivroz, G. Courtois, R. Döffinger, and all members of the Laboratory of Human Genetics of Infectious Diseases for helpful discussions. We are particularly grateful to the families for agreeing to participate in this study. We thank T. Leclerc, M. Courat, and C. Bidalled for excellent technical and secretarial assistance. A. Plebani and L. Notarangelo thank the *Centro per le Immunodeficienze Primitive "Mario di Martino"*.

O. Filipe-Santos was supported by *Fundação para a Ciência e Tecnologia*, Portugal; J. Bustamante was supported by the Fondation Schlumberger and INSERM. The Laboratory of Human Genetics of Infectious Diseases is supported in part by grants from the Schlumberger and BNP Paribas Foundations, the March of Dimes, and by EU grant QLK2-CT-2002-00846. S.M. Holland and M. Haverkamp acknowledge the support of the intramural program of the National Institute of Allergy and Infectious Diseases, National Institutes of Health. Studies by E. Vinolo, F. Agou, M. Véron, and A. Israël were supported by the *Association pour la Recherche contre le Cancer* and the *Cancéropôle Ile de France*. J.-L. Casanova is an International Scholar of the Howard Hughes Medical Institute.

The authors have no conflicting interests.

Submitted: 9 January 2006
Accepted: 25 May 2006

REFERENCES

1. Holland, S.M., E.M. Eisenstein, D.B. Kuhns, M.L. Turner, T.A. Fleisher, W. Strober, and J.I. Gallin. 1994. Treatment of refractory disseminated nontuberculous mycobacterial infection with interferon γ. A preliminary report. *N. Engl. J. Med.* 330:1348–1355.
2. Levin, M., M.J. Newport, S. D'Souza, P. Kalabalikis, I.N. Brown, H.M. Lenicker, P.V. Agius, E.G. Davies, A. Thrasher, N. Klein, and J. Blackwell. 1995. Familial disseminated atypical mycobacterial infection in childhood: a human mycobacterial susceptibility gene? *Lancet.* 345:79–83.
3. Casanova, J.L., E. Jouanguy, S. Lamhamedi, S. Blanche, and A. Fischer. 1995. Immunological conditions of children with BCG disseminated infection. *Lancet.* 346:581.
4. Casanova, J.L., and L. Abel. 2002. Genetic dissection of immunity to mycobacteria: the human model. *Annu. Rev. Immunol.* 20:581–620.
5. Alcais, A., C. Fieschi, L. Abel, and J.L. Casanova. 2005. Tuberculosis in children and adults: two distinct genetic diseases. *J. Exp. Med.* 202:1617–1621.
6. Newport, M.J., C.M. Huxley, S. Huston, C.M. Hawrylowicz, B.A. Oostra, R. Williamson, and M. Levin. 1996. A mutation in the interferon-γ-receptor gene and susceptibility to mycobacterial infection. *N. Engl. J. Med.* 335:1941–1949.
7. Jouanguy, E., F. Altare, S. Lamhamedi, P. Revy, J.F. Emile, M. Newport, M. Levin, S. Blanche, E. Seboun, A. Fischer, and J.L. Casanova. 1996. Interferon-γ-receptor deficiency in an infant with fatal bacille Calmette-Guerin infection. *N. Engl. J. Med.* 335: 1956–1961.
8. Dorman, S.E., and S.M. Holland. 1998. Mutation in the signal-transducing chain of the interferon-γ receptor and susceptibility to mycobacterial infection. *J. Clin. Invest.* 101:2364–2369.
9. Altare, F., D. Lammas, P. Revy, E. Jouanguy, R. Doffinger, S. Lamhamedi, P. Drysdale, D. Scheel-Toellner, J. Girdlestone, P. Darbyshire, et al. 1998. Inherited interleukin 12 deficiency in a child with bacille Calmette-Guerin and Salmonella enteritidis disseminated infection. *J. Clin. Invest.* 102:2035–2040.
10. Altare, F., A. Durandy, D. Lammas, J.F. Emile, S. Lamhamedi, F. Le Deist, P. Drysdale, E. Jouanguy, R. Döffinger, F. Bernaudin, et al. 1998. Impairment of mycobacterial immunity in human interleukin-12 receptor deficiency. *Science.* 280:1432–1435.
11. de Jong, R., F. Altare, I.A. Haagen, D.G. Elferink, T. Boer, P.J. van Breda Vriesman, P.J. Kabel, J.M. Draaisma, J.T. van Dissel, F.P. Kroon, et al. 1998. Severe mycobacterial and Salmonella infections in interleukin-12 receptor-deficient patients. *Science.* 280:1435–1438.
12. Jouanguy, E., S. Lamhamedi-Cherradi, F. Altare, M.C. Fondaneche, D. Tuerlinckx, S. Blanche, J.F. Emile, J.L. Gaillard, R. Schreiber, M. Levin, et al. 1997. Partial interferon-γ receptor 1 deficiency in a child with tuberculoid bacillus Calmette-Guerin infection and a sibling with clinical tuberculosis. *J. Clin. Invest.* 100:2658–2664.
13. Döffinger, R., E. Jouanguy, S. Dupuis, M.C. Fondanèche, J.L. Stéphan, J.F. Emile, S. Lamhamedi, F. Altare, A. Pallier, G. Barcenas-Morales, et al. 2000. Partial interferon γ receptor signalling chain deficiency in a patient with bacille Calmette-Guérin and Mycobacterium abscessus infection. *J. Infect. Dis.* 181:379–384.

14. Jouanguy, E., S. Dupuis, A. Pallier, R. Döffinger, M.C. Fondanèche, S. Lamhamedi-Cherradi, F. Altare, J.F. Emile, P. Lutz, P. Bordigoni, et al. 2000. In a novel form of complete IFNγR1 deficiency, cell-surface receptors fail to bind IFNγ. *J. Clin. Invest.* 105:1429–1436.
15. Vogt, G., A. Chapgier, K. Yang, N. Chuzhanova, J. Feinberg, C. Fieschi, S. Boisson-Dupuis, A. Alcais, O. Filipe-Santos, J. Bustamante, et al. 2005. Gains of glycosylation comprise an unexpectedly large group of pathogenic mutations. *Nat. Genet.* 37:692–700.
16. Fieschi, C., M. Bosticardo, L. de Beaucoudrey, S. Boisson-Dupuis, J. Feinberg, O.F. Santos, J. Bustamante, J. Levy, F. Candotti, and J.L. Casanova. 2004. A novel form of complete IL-12/IL-23 receptor beta1 deficiency with cell surface-expressed nonfunctional receptors. *Blood.* 104:2095–2101.
17. Jouanguy, E., S. Lamhamedi-Cherradi, D. Lammas, S.E. Dorman, M.C. Fondaneche, S. Dupuis, R. Doffinger, F. Altare, J. Girdlestone, J.F. Emile, et al. 1999. A human IFNGR1 small deletion hotspot associated with dominant susceptibility to mycobacterial infection. *Nat. Genet.* 21:370–378.
18. Dupuis, S., C. Dargemont, C. Fieschi, N. Thomassin, S. Rosenzweig, J. Harris, S.M. Holland, R.D. Schreiber, and J.L. Casanova. 2001. Impairment of mycobacterial but not viral immunity by a germline human STAT1 mutation. *Science.* 293:300–303.
19. Rosenzweig, S.D., S.E. Dorman, G. Uzel, S. Shaw, A. Scurlock, M.R. Brown, R.H. Buckley, and S.M. Holland. 2004. A novel mutation in IFN-γ receptor 2 with dominant negative activity: biological consequences of homozygous and heterozygous states. *J. Immunol.* 173:4000–4008.
20. Nedorost, S.T., B. Elewski, J.W. Tomford, and C. Camisa. 1991. Rosacea-like lesions due to familial *Mycobacterium avium*-intracellulare infection. *Int. J. Dermatol.* 30:491–497.
21. Frucht, D.M., and S.M. Holland. 1996. Defective monocyte costimulation for IFN-γ production in familial disseminated *Mycobacterium avium* complex infection: abnormal IL-12 regulation. *J. Immunol.* 157:411–416.
22. Frucht, D.M., D.I. Sandberg, M.R. Brown, S.M. Gerstberger, and S.M. Holland. 1999. IL-12-independent costimulation pathways for interferon-γ production in familial disseminated *Mycobacterium avium* complex infection. *Clin. Immunol.* 91:234–241.
23. Zonana, J., M.E. Elder, L.C. Schneider, S.J. Orlow, C. Moss, M. Golabi, S.K. Shapira, P.A. Farndon, D.W. Wara, S.A. Emmal, and B.M. Ferguson. 2000. A novel X-linked disorder of immune deficiency and hypohidrotic ectodermal dysplasia is allelic to incontinentia pigmenti and due to mutations in IKK-γ (NEMO). *Am. J. Hum. Genet.* 67:1555–1562.
24. Doffinger, R., A. Smahi, C. Bessia, F. Geissmann, J. Feinberg, A. Durandy, C. Bodemer, S. Kenwrick, S. Dupuis-Girod, S. Blanche, et al. 2001. X-linked anhidrotic ectodermal dysplasia with immunodeficiency is caused by impaired NF-κB signaling. *Nat. Genet.* 27:277–285.
25. Jain, A., C.A. Ma, S. Liu, M. Brown, J. Cohen, and W. Strober. 2001. Specific missense mutations in NEMO result in hyper-IgM syndrome with hypohydrotic ectodermal dysplasia. *Nat. Immunol.* 2:223–228.
26. Ku, C.L., S. Dupuis-Girod, A.M. Dittrich, J. Bustamante, O.F. Santos, I. Schulze, Y. Bertrand, G. Couly, C. Bodemer, X. Bossuyt, et al. 2005. NEMO mutations in 2 unrelated boys with severe infections and conical teeth. *Pediatrics.* 115:615–619.
27. Smahi, A., G. Courtois, P. Vabres, S. Yamaoka, S. Heuertz, A. Munnich, A. Israel, N.S. Heiss, S.M. Klauck, P. Kioschis, et al. 2000. Genomic rearrangement in NEMO impairs NF-κB activation and is a cause of incontinentia pigmenti. The International Incontinentia Pigmenti (IP) Consortium. *Nature.* 405:466–472.
28. Huang, G.J., Z.Q. Zhang, and D.Y. Jin. 2002. Stimulation of IKK-γ oligomerization by the human T-cell leukemia virus oncoprotein Tax. *FEBS Lett.* 531:494–498.
29. Agou, F., F. Ye, S. Goffinont, G. Courtois, S. Yamaoka, A. Israel, and M. Veron. 2002. NEMO trimerizes through its coiled-coil C-terminal domain. *J. Biol. Chem.* 277:17464–17475.
30. Agou, F., F. Traincard, E. Vinolo, G. Courtois, S. Yamaoka, A. Israel, and M. Veron. 2004. The trimerization domain of NEMO is composed of the interacting C-terminal CC2 and LZ coiled-coil subdomains. *J. Biol. Chem.* 279:27861–27869.
31. Chan, D.C., D. Fass, J.M. Berger, and P.S. Kim. 1997. Core structure of gp41 from the HIV envelope glycoprotein. *Cell.* 89:263–273.
32. Nishikomori, R., H. Akutagawa, K. Maruyama, M. Nakata-Hizume, K. Ohmori, K. Mizuno, A. Yachie, T. Yasumi, T. Kusunoki, T. Heike, and T. Nakahata. 2004. X-linked ectodermal dysplasia and immunodeficiency caused by reversion mosaicism of NEMO reveals a critical role for NEMO in human T-cell development and/or survival. *Blood.* 103:4565–4572.
33. Fieschi, C., S. Dupuis, E. Catherinot, J. Feinberg, J. Bustamante, A. Breiman, F. Altare, R. Baretto, F. Le Deist, S. Kayal, et al. 2003. Low penetrance, broad resistance, and favorable outcome of interleukin 12 receptor β1 deficiency: medical and immunological implications. *J. Exp. Med.* 197:527–535.
34. Shu, U., M. Kiniwa, C.Y. Wu, C. Maliszewski, N. Vezzio, J. Hakimi, M. Gately, and G. Delespesse. 1995. Activated T cells induce interleukin-12 production by monocytes via CD40-CD40 ligand interaction. *Eur. J. Immunol.* 25:1125–1128.
35. Stuber, E., W. Strober, and M. Neurath. 1996. Blocking the CD40L–CD40 interaction in vivo specifically prevents the priming of T helper 1 cells through the inhibition of interleukin 12 secretion. *J. Exp. Med.* 183:693–698.
36. Cella, M., D. Scheidegger, K. Palmer-Lehmann, P. Lane, A. Lanzavecchia, and G. Alber. 1996. Ligation of CD40 on dendritic cells triggers production of high levels of interleukin-12 and enhances T cell stimulatory capacity: T-T help via APC activation. *J. Exp. Med.* 184:747–752.
37. Takenaka, H., S. Maruo, N. Yamamoto, M. Wysocka, S. Ono, M. Kobayashi, H. Yagita, K. Okumura, T. Hamaoka, G. Trinchieri, and H. Fujiwara. 1997. Regulation of T cell-dependent and -independent IL-12 production by the three Th2-type cytokines IL-10, IL-6, and IL-4. *J. Leukoc. Biol.* 61:80–87.
38. Ferrari, S., and A. Plebani. 2002. Cross-talk between CD40 and CD40L: lessons from primary immune deficiencies. *Curr. Opin. Allergy Clin. Immunol.* 2:489–494.
39. Fontana, S., D. Moratto, S. Mangal, M. De Francesco, W. Vermi, S. Ferrari, F. Facchetti, N. Kutukculer, C. Fiorini, M. Duse, et al. 2003. Functional defects of dendritic cells in patients with CD40 deficiency. *Blood.* 102:4099–4106.
40. Peng, X., A. Kasran, P.A. Warmerdam, M. de Boer, and J.L. Ceuppens. 1996. Accessory signaling by CD40 for T cell activation: induction of Th1 and Th2 cytokines and synergy with interleukin-12 for interferon-γ production. *Eur. J. Immunol.* 26:1621–1627.
41. Ouaaz, F., J. Arron, Y. Zheng, Y. Choi, and A.A. Beg. 2002. Dendritic cell development and survival require distinct NF-κB subunits. *Immunity.* 16:257–270.
42. Mason, N., J. Aliberti, J.C. Caamano, H.C. Liou, and C.A. Hunter. 2002. Cutting edge: identification of c-Rel-dependent and -independent pathways of IL-12 production during infectious and inflammatory stimuli. *J. Immunol.* 168:2590–2594.
43. Puel, A., J. Reichenbach, J. Bustamante, C.L. Ku, J. Feinberg, R. Doffinger, M. Bonnet, O. Filipe-Santos, L. Beaucoudrey, A. Durandy, et al. 2006. The NEMO mutation creating the most-upstream premature stop codon is hypomorphic because of a reinitiation of translation. *Am. J. Hum. Genet.* 78:691–701.
44. Florido, M., A.S. Goncalves, M.S. Gomes, and R. Appelberg. 2004. CD40 is required for the optimal induction of protective immunity to *Mycobacterium avium*. *Immunology.* 111:323–327.
45. Hayashi, T., S.P. Rao, P.R. Meylan, R.S. Kornbluth, and A. Catanzaro. 1999. Role of CD40 ligand in *Mycobacterium avium* infection. *Infect. Immun.* 67:3558–3565.
46. Campos-Neto, A., P. Ovendale, T. Bement, T.A. Koppi, W.C. Fanslow, M.A. Rossi, and M.R. Alderson. 1998. CD40 ligand is not essential for the development of cell-mediated immunity and resistance to *Mycobacterium tuberculosis*. *J. Immunol.* 160:2037–2041.
47. Lazarevic, V., A.J. Myers, C.A. Scanga, and J.L. Flynn. 2003. CD40, but not CD40L, is required for the optimal priming of T cells and control of aerosol *M. tuberculosis* infection. *Immunity.* 19:823–835.

48. Levy, J., T. Espanol-Boren, C. Thomas, A. Fischer, P. Tovo, P. Bordigoni, I. Resnick, A. Fasth, M. Baer, L. Gomez, et al. 1997. Clinical spectrum of X-linked hyper-IgM syndrome. *J. Pediatr.* 131:47–54.
49. Kindler, V., A.P. Sappino, G.E. Grau, P.F. Piguet, and P. Vassalli. 1989. The inducing role of tumor necrosis factor in the development of bactericidal granulomas during BCG infection. *Cell.* 56:731–740.
50. Casanova, J.L., and L. Abel. 2004. The human model: a genetic dissection of immunity to infection in natural conditions. *Nat. Rev. Immunol.* 4:55–66.
51. Aradhya, S., G. Courtois, A. Rajkovic, R. Lewis, M. Levy, A. Israel, and D. Nelson. 2001. Atypical forms of incontinentia pigmenti in male individuals result from mutations of a cytosine tract in exon 10 of NEMO (IKK-γ). *Am. J. Hum. Genet.* 68:765–771.
52. Orange, J.S., S.R. Brodeur, A. Jain, F.A. Bonilla, L.C. Schneider, R. Kretschmer, S. Nurko, W.L. Rasmussen, J.R. Kohler, S.E. Gellis, et al. 2002. Deficient natural killer cell cytotoxicity in patients with IKK-γ/NEMO mutations. *J. Clin. Invest.* 109:1501–1509.
53. Dupuis-Girod, S., N. Corradini, S. Hadj-Rabia, J.C. Fournet, L. Faivre, F. Le Deist, P. Durand, R. Doffinger, A. Smahi, A. Israel, et al. 2002. Osteopetrosis, lymphedema, anhidrotic ectodermal dysplasia, and immunodeficiency in a boy and incontinentia pigmenti in his mother. *Pediatrics.* 109:e97.
54. Mansour, S., H. Woffendin, S. Mitton, I. Jeffery, T. Jakins, S. Kenwrick, and V.A. Murday. 2001. Incontinentia pigmenti in a surviving male is accompanied by hypohidrotic ectodermal dysplasia and recurrent infection. *Am. J. Med. Genet.* 99:172–177.
55. Jain, A., C.A. Ma, E. Lopez-Granados, G. Means, W. Brady, J.S. Orange, S. Liu, S. Holland, and J.M. Derry. 2004. Specific NEMO mutations impair CD40-mediated c-Rel activation and B cell terminal differentiation. *J. Clin. Invest.* 114:1593–1602.